

# Engineering the coupling between Majorana bound states

Z. C. Shi<sup>1,2</sup>, X. Q. Shao<sup>3</sup>, Y. Xia<sup>1,2,\*</sup>, and X. X. Yi<sup>3,†</sup>

<sup>1</sup> Department of Physics, Fuzhou University, Fuzhou 350002, China

<sup>2</sup> Fujian Key Laboratory of Quantum Information and Quantum Optics (Fuzhou University), Fuzhou 350116, China

<sup>3</sup> Center for Quantum Sciences and School of Physics, Northeast Normal University, Changchun 130024, China

We study the coupling between Majorana bound states (CMBS), which is mediated by a topologically trivial chain in the presence of pairing coupling and long-range coupling. The results show that CMBS can be enhanced by the pairing coupling and long-range coupling of the trivial chain. When driving the trivial chain by periodic driving field, we deduce the analytical expressions of CMBS in the high-frequency limit, and demonstrate that CMBS can be modulated by the frequency and amplitude of driving field. Finally we exhibit the application of tunable CMBS in realizing quantum logic gates.

## I. INTRODUCTION

Topological quantum computation [1, 2], immune to certain types of noise, has attracted much attention since it was proposed and becomes active again in recent years due to the enormous progress in experiments. The gates used in topological quantum computation is often conducted by creating quasi-particles, braiding them, and measuring their states. For quasi-particles, two well-known types are Fibonacci anyons and Ising anyons [Majorana bound states (MBSs)]. The former are capable of offering universal topological quantum computation, while the latter can not form an universal set of gates by only braiding operations. So non-topologically protected gates have to be introduced in the MBSs-based computation, which always requires coupling between Majorana bound states (CMBS). Although it makes some breakthrough to pursue MBSs in theories [3–10] and experiments [11–16], the question how to couple two MBSs is barely explored.

Recently, Schmidt and his co-workers [17, 18] presented proposals to couple MBSs by putting the system into a microwave cavity, where the microwave field can effectively drive population transfer between MBSs. The authors found that if the microwave frequency approaches the band gap of the topologically trivial region, CMBS is exponentially enhanced. In other words, CMBS is controllable by modulating microwave frequency or changing the number of photons in the cavity. However, CMBS is relatively small in this system and one cannot very easily control the parameters to realize unitary operation of qubit formed by MBSs. In this work, we study how to enhance CMBS by the pairing coupling and long-range coupling in the central chain, and CMBS can be modulated by periodic driving field. In particular the universal Majorana qubit rotation (UMQR) can be implemented by simply controlling the tunable local gate voltage (TLGV)

with square-wave form.

The paper is organized as follows. In Sec. II we first briefly review the Kitaev model and calculate CMBS in presence of pairing coupling of the central chain. In Sec. III we explore the enhancement of CMBS when there exist pairing couplings at the boundaries and long-range coupling in the trivial chain. In Sec. IV we develop a scheme to control CMBS by modulating the amplitude or the frequency of driving field. Sec. V is devoted to discussions and conclusions.

## II. CMBS INDUCED BY THE TRIVIAL CHAIN

Consider an inhomogeneous Kitaev chain [19] which can be divided into three homogeneous parts. The total Hamiltonian of the whole chain reads

$$H_{total} = H_l + H_c + H_r + H_{lc} + H_{rc}, \quad (1)$$

where  $H_l$  ( $H_r$ ) denotes the Hamiltonian of left (right) chain with sites from  $-N_1$  ( $N+1$ ) to  $-1$  ( $N_2$ ), and  $H_c$  represents the Hamiltonian of central chain with sites from 0 to  $N$ .  $H_{lc}$  ( $H_{rc}$ ) denotes the Hamiltonian of the coupling between the left (right) chain and the central chain. To be specific the Hamiltonian of the three homogeneous Kitaev chains is expressed as

$$H_\nu = \sum_{n=M_\nu}^{M'_\nu} \mu_\nu a_n^\dagger a_n - \sum_{n=M_\nu}^{M'_\nu-1} \left( \frac{t_\nu}{2} a_n^\dagger a_{n+1} + \frac{\Delta_\nu e^{i\phi_\nu}}{2} a_n^\dagger a_{n+1}^\dagger + h.c. \right), \quad (2)$$

where  $a_n$  and  $a_n^\dagger$  are the spinless fermion creation and annihilation operators at site  $n$  with chemical potential  $\mu_\nu$  ( $\nu = l, c, r$ ).  $M_\nu = \{-N_1, 0, N+1\}$  and  $M'_\nu = \{-1, N, N_2\}$  label the beginning and end sites of the left, central, and right chain, respectively.  $t_\nu$  and  $\Delta_\nu e^{i\phi_\nu}$  are the hopping and pairing amplitudes, respectively. Since the phase of the pairing amplitude can be removed from the Hamiltonian by a gauge transformation, we here and hereafter assume both  $t_\nu$  and  $\Delta_\nu$  to be real.

\*xia-208@163.com  
†yixx@nenu.edu.cn

Physically, the Kitaev model can be exactly mapped into the spin- $\frac{1}{2}$  chain with XY interactions [20], the quantum system of the semiconductor nanowire proximity coupling to a  $s$ -wave superconductor [21, 22], or the atomic chains [23, 24]. This paradigm model shows plentiful fascinating topological properties and there are two distinct phases, i.e., the topologically trivial and nontrivial phases. The critical points lie at  $\frac{\mu_\nu}{t_\nu} = 1$  and  $\Delta_\nu = 0$  [19].

By choosing  $\mu_l = \mu_r = 0$  (the chemical potential can be modulated by TLGV  $V_i$  shown in Fig. 1) and  $\Delta_l = \Delta_r = t_l = t_r$  for the left and right chains, both chains are in the topologically nontrivial phase. As a result there exist MBSs at the ends of both chains, depicted by the stars in Fig. 1. If one defines Majorana operators

$$\gamma_n = a_n + a_n^\dagger, \quad \gamma'_n = i(a_n^\dagger - a_n), \quad n = -N_1, \dots, N_2, \quad (3)$$

after substituting them into Eq.(2), the Hamiltonian of left (right) chain becomes

$$H_\nu = i \frac{t_\nu}{2} \sum_{n=M_\nu}^{M'_\nu-1} \gamma_n \gamma'_{n+1}, \quad \nu = l, r. \quad (4)$$

Clearly, the Majorana operators  $\gamma_n$  and  $\gamma'_{n+1}$  are coupled with different sites. In particular the Majorana operators  $\gamma'_{N_1} = i(a_{-N_1}^\dagger - a_{-N_1})$ ,  $\gamma_{-1} = a_{-1} + a_{-1}^\dagger$ ,  $\gamma'_{N_2+1} = i(a_{N_2+1}^\dagger - a_{N_2+1})$ , and  $\gamma_{N_2} = a_{N_2} + a_{N_2}^\dagger$  do not appear in Eq. (4), leading to the emergence of four MBSs in the chains. Since the four MBSs are decoupled to the remaining sites and only locate at the end of both left and right chains, we can ignore the Hamiltonian of the remaining sites when studying CMBS.

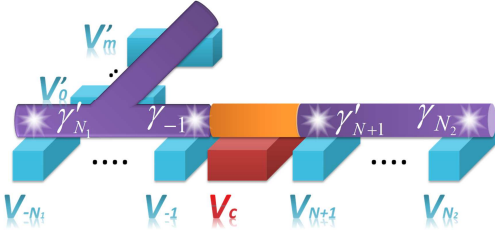


FIG. 1: Schematic illustration for realizing universal Majorana qubit rotation in the Kitaev chain. There is a direct relationship between the Kitaev model and the solid state system in the low-density limit (for details, see Refs. [18, 25]). The braiding operation can be realized in the T-junction on the left chain by adiabatically controlling TLGV  $V_i$  in sequence, and the CMBS can be modulated by the voltage  $V_c$ .

To couple MBSs  $\gamma_{-1}$  and  $\gamma'_{N_2+1}$ , the parameters  $\{\mu_c, t_c, \Delta_c\}$  should be chosen to guarantee the central chain is in topologically trivial phase. Otherwise the MBSs  $\gamma_{-1}$  and  $\gamma'_{N_2+1}$  would disappear in this inhomogeneous chain. As we just consider the nearest-neighbour interactions in Eq. (2), only the MBSs  $\gamma_{-1}$  and  $\gamma'_{N_2+1}$  can

be coupled to the central chain. So the Hamiltonian of interest is given by [26]

$$\begin{aligned} H_i &= H_c + H_{lc} + H_{rc}, \\ H_{lc} &= -\frac{t_1}{2} \gamma_{-1} (a_0 - a_0^\dagger), \\ H_{rc} &= -\frac{it_2}{2} (a_N + a_N^\dagger) \gamma'_{N_2+1}. \end{aligned} \quad (5)$$

In order to obtain the energy spectrum of the central chain, it is convenient to carry out Fourier transform  $a_n = \frac{1}{\sqrt{N+1}} \sum_k a_k e^{ikn}$  by imposing periodic boundary condition (we have set the lattice spacing to be unit and Fourier transform will be precise when the number of sites is large,  $N \sim \infty$ ). The validity of Fourier transform is also verified by numerical calculations in Fig. 2. The Hamiltonian of the central chain now becomes

$$H_c = \sum_k (\mu_c - t_c \cos k) a_k^\dagger a_k - i \Delta_c \sin k a_k^\dagger a_{-k}^\dagger + h.c. \quad (6)$$

One can rewrite the above Hamiltonian in a normal Bogoliubov-de Gennes (BdG) form by defining a two component operator  $A_k^\dagger = [a_k^\dagger, a_{-k}]$ , i.e.,

$$H_c = \sum_k A_k^\dagger \mathcal{H}_k A_k, \quad \mathcal{H}_k = \begin{pmatrix} h_z & -ih_y \\ ih_y & -h_z \end{pmatrix}, \quad (7)$$

where  $h_z = \mu_c - t_c \cos k$  and  $h_y = \Delta_c \sin k$ . Consequently the Hamiltonian is further simplified as (up to a constant)

$$H_c = \sum_k E_k b_k^\dagger b_k, \quad (8)$$

where the quasi-particle operator  $b_k$  is defined as  $b_k = u_k a_k - v_k a_{-k}^\dagger$  and the energy spectrum of the central chain is given by  $E_k = \sqrt{(\mu_c - t_c \cos k)^2 + \Delta_c^2 \sin^2 k}$ ,  $|u_k| = \sqrt{\frac{1}{2}(1 + \frac{\mu_c - t_c \cos k}{E_k})}$ ,  $|v_k| = \sqrt{\frac{1}{2}(1 - \frac{\mu_c - t_c \cos k}{E_k})}$ . Using the above notations, we can rewrite the Hamiltonian of interest more explicitly as

$$\begin{aligned} H_i &= \sum_k E_k b_k^\dagger b_k - \sum_k \frac{t_1}{2} \gamma_{-1} [(u_k + v_k) b_k^\dagger - (u_k^* + v_k^*) b_k] \\ &\quad - \sum_k \frac{t_2}{2} [e^{-ikN} (u_k - v_k) b_k^\dagger + e^{ikN} (u_k^* - v_k^*) b_k] \gamma'_{N_2+1}. \end{aligned} \quad (9)$$

Since we are particularly interested in the low-energy dynamics of system, we apply Schrieffer-Wolff transformation [27] to eliminate high-energy spectrum. We denote the first term in Eq. (9) by  $\mathcal{H}_0$  and the remaining terms by  $\mathcal{H}_1$ . By choosing the unitary transformation  $\mathcal{S}$  to satisfy the relation  $[\mathcal{H}_0, \mathcal{S}] = \mathcal{H}_1$ , one has

$$\begin{aligned} \mathcal{S} &= \sum_k \frac{t_1 (u_k + v_k) \gamma_{-1} b_k - t_1 (u_k^* + v_k^*) b_k^\dagger \gamma_{-1}}{2E_k} \\ &\quad + \sum_k \frac{t_2 e^{ikN} (u_k - v_k) \gamma'_{N_2+1} b_k - t_2 e^{-ikN} (u_k^* - v_k^*) b_k^\dagger \gamma'_{N_2+1}}{2E_k}. \end{aligned} \quad (10)$$

Making use of the Baker-Hausdorff formula:  $e^{-S}H_i e^S = H_i + [H_i, S] + \frac{1}{2}[[H_i, S], S] + \dots$ , and keeping the terms up to first order, we obtain an effective Hamiltonian between the adjacent MBSs  $\gamma_{-1}$  and  $\gamma'_{N+1}$ , i.e.,

$$H_{0N} = i\epsilon\gamma_{-1}\gamma'_{N+1}, \quad \epsilon = \frac{t_1 t_2}{\sqrt{\mu_c^2 + \Delta_c^2 - t_c^2}} e^{-N/\epsilon_0}. \quad (11)$$

Here  $\epsilon_0$  is the coherence length,  $\epsilon_0^{-1} = \ln \frac{\Delta_c - t_c}{\sqrt{\mu_c^2 + \Delta_c^2 - t_c^2} - \mu_c}$ .  $\epsilon$  represents the amplitude for the MBSs tunneling across the central chain. Eq. (11) demonstrates that the effective coupling between MBSs  $\gamma_{-1}$  and  $\gamma'_{N+1}$  can be induced by the central chain. This is a virtual co-tunneling process since there exists energy gap in the central chain and real electrons and holes cannot tunnel from one MBS to another. In addition, the coupling strength  $\epsilon$  depends exponentially on the length  $N$ . When  $N$  is large enough, the degeneracy energies of MBSs are in the energy gap, which is the reason why MBSs are topologically protected. In Fig. 2(a), we plot the coupling strength  $\epsilon$  versus the chemical potential  $\mu_c$  with different pairing amplitudes  $\Delta_c$ . It is readily observed that the analytical solutions of  $\epsilon$  are in well agreement with the numerical solutions when the chemical potential is large enough and the coupling strength  $\epsilon$  decreases with the increasing of chemical potential  $\mu_c$ , reminiscent of the results where the Majorana qubit setup is placed in a microwave cavity [18]. However, one also finds that the coupling strength  $\epsilon$  is enhanced by the pairing amplitude  $\Delta_c$  of the central chain, which is not mentioned in Ref. [18]. Physically, it originates from the fact that large pairing amplitude  $\Delta_c$  would broaden the energy spectrum [cf.  $E_k$  in Eq. (8)], leading to more quasi-particles participating in the co-tunneling process. As a result the coherence length  $\epsilon_0$  also increases accordingly, which is verified in Fig. 2(b).

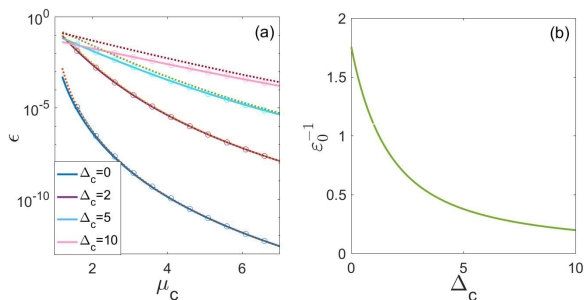


FIG. 2: (a) The coupling strength  $\epsilon$  as a function of the chemical potential  $\mu_c$  with different pairing couplings  $\Delta_c$ ,  $N = 10$ . The circle and solid lines are exact solutions by numerically diagonalizing the Hamiltonian (1) with and without periodic boundary condition respectively, indicating no obvious difference by imposing periodic boundary condition. The dot line is approximate analytical solutions described by Eq. (11). All parameters are in units of hopping amplitude, i.e.,  $t_1 = t_2 = t_l = t_r = t_c = 1$ . (b) The coherence length versus the pairing amplitude with  $\mu_c = 3$ .

### III. THE ENHANCEMENT OF CMBS

In Eq. (5), we just consider the hopping coupling at the boundaries between left (right) chain and central chain. When existing pairing coupling at the boundaries, the Hamiltonian of interest becomes

$$\begin{aligned} H_i &= H_c + H_{lc} + H_{rc}, \\ H_{lc} &= -\frac{t_1}{2}\gamma_{-1}(a_0 - a_0^\dagger) - \frac{\Delta_1}{2}(a_{-1}^\dagger a_0^\dagger - a_{-1}a_0), \\ H_{rc} &= -\frac{it_2}{2}(a_N + a_N^\dagger)\gamma'_{N+1} - \frac{\Delta_2}{2}(a_N^\dagger a_{N+1}^\dagger - a_N a_{N+1}), \end{aligned} \quad (12)$$

where  $H_c$  is the same as in Eq. (5). By using the Majorana operators representation in Eq. (3), the Hamiltonian can be rewritten as,

$$\begin{aligned} H_{lc} &= -\frac{t_1 + \Delta_1}{2}\gamma_{-1}(a_0 - a_0^\dagger) + \frac{i\Delta_1}{2}\gamma'_{-1}(a_0 + a_0^\dagger), \\ H_{rc} &= -\frac{i(t_2 + \Delta_2)}{2}(a_N + a_N^\dagger)\gamma'_{N+1} + \frac{\Delta_2}{2}(a_N - a_N^\dagger)\gamma_{N+1}. \end{aligned} \quad (13)$$

The second term in the Hamiltonian  $H_{lc}$  ( $H_{rc}$ ) can be ignored if we only consider CMBS, but this term affects the spatial distribution of the MBSs  $\gamma_{-1}$  and  $\gamma'_{N+1}$ . Hence the effective hopping coupling between the central chain and the left (right) chain is enhanced as  $\frac{t_1 + \Delta_1}{2}$  ( $\frac{t_2 + \Delta_2}{2}$ ). As a result, the value of coupling strength  $\epsilon$  increases in the existence of pairing coupling at the boundaries.

Figs. 3(a)-(b) demonstrate the coupling strength  $\epsilon$  as a function of the pairing amplitude  $\Delta_c$ . It is observed that the analytical solutions are in well agreement with the numerical solutions when  $\mu_c$  is large enough, and the coupling strength  $\epsilon$  can reach a relatively high value even though the central chain is long. Note that CMBS would in turn affect the spatial distribution of MBSs  $\gamma_{-1}$  and  $\gamma'_{N+1}$ . Especially, the spatial distribution of MBSs will be greatly modified when the coupling strength  $\epsilon$  is large, as shown in Figs. 3(c)-(e).

On the other hand, when the central chain exists long-range coupling [e.g., the next-nearest-neighbor (NNN) couplings], the Hamiltonian can be described by

$$\begin{aligned} H_c &= \sum_{n=0}^N \mu_c a_n^\dagger a_n - \sum_{m=1}^2 \sum_{n=0}^{N-m} \left( \frac{t_{cm}}{2} a_n^\dagger a_{n+m} \right. \\ &\quad \left. + \frac{\Delta_{cm}}{2} a_n^\dagger a_{n+m}^\dagger + h.c. \right). \end{aligned} \quad (14)$$

Physically, with the help of Raman laser, this model can be realized by the system of fermi atoms trapping in optical lattice with zigzag structure and coupling to a 3D Bose-Einstein condensate (BEC) reservoir, as shown in Fig. 4. The relative strength of hopping amplitudes  $t_{c1}$  and  $t_{c2}$  can be modulated by changing the zigzag geometry. For details, we refer readers to Ref. [28, 29]. In

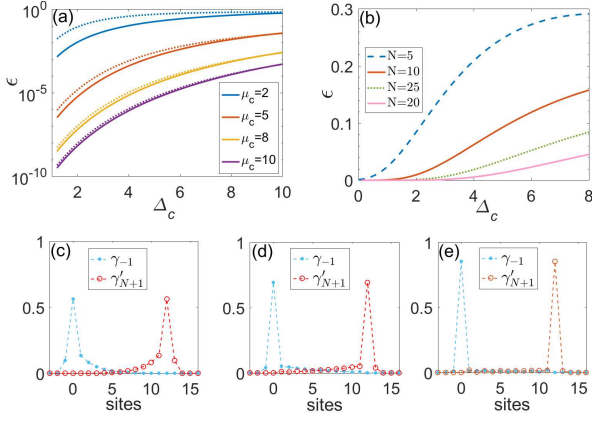


FIG. 3: (a) The coupling strength  $\epsilon$  as a function of the pairing amplitude  $\Delta_c$  with different chemical potentials  $\mu_c$ ,  $N = 10$ . The solid line and dot line denote the exact numerical solutions and the approximate analytical solutions respectively, where the hopping amplitude  $t_1 t_2$  are revised as  $(t_1 + \Delta_1)(t_2 + \Delta_2)$ . All parameters are chosen in units of hopping amplitude in the central chain.  $\Delta_1 = \Delta_2 = 5$ . (b) The exact numerical solutions of coupling strength  $\epsilon$  versus the pairing amplitude  $\Delta_c$  when  $\mu_c = 2$ ,  $\Delta_1 = \Delta_2 = 1$ . (c)-(e) The spatial density distribution of MBSs  $\gamma_{-1}$  and  $\gamma'_{N+1}$  versus different coupling strength  $\epsilon$ . (c)  $\epsilon = 0.0337$ . (d)  $\epsilon = 0.2055$ . (e)  $\epsilon = 0.2519$ .

this case, the coupling Hamiltonian at the boundaries between left (right) chain and central chain reads

$$\begin{aligned}
 H_{lc} &= -\frac{t_1}{2}\gamma_{-1}(a_0 - a_0^\dagger) - \frac{t'_1}{2}\gamma_{-1}(a_1 - a_1^\dagger), \\
 H_{rc} &= -\frac{it_2}{2}(a_N + a_N^\dagger)\gamma'_{N+1} - \frac{it'_2}{2}(a_{N-1} + a_{N-1}^\dagger)\gamma'_{N+1}.
 \end{aligned}
 \tag{15}$$

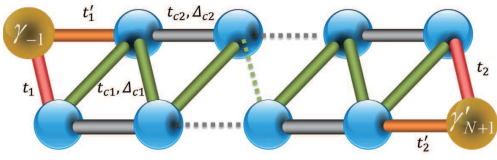


FIG. 4: The zigzag structure of the Kitaev chain which can be realized in optical lattices.

Following the similar derivation procedures in Eqs. (5)-(11), one can estimate the effective Hamiltonian of CMBS,

$$\begin{aligned}
 H'_{0N} &= i\epsilon\gamma_{-1}\gamma'_{N+1} \\
 \epsilon &= \sum_k \left| \lim_{z \rightarrow z_k} (z - z_k) \frac{2(t_1 z + t'_1)(t_2 z + t'_2)z^{N-1}}{\prod_{i=1}^4 (z - z_i)} \right|, \\
 z_k &\in \left\{ z_i \mid |z_i| < 1, i = 1, 2, 3, 4 \right\},
 \end{aligned}
 \tag{16}$$

where  $z_i$  ( $i = 1, 2, 3, 4$ ) is the root of the quartic equation  $(\Delta_{c2} - t_{c2})z^4 + (\Delta_{c1} - t_{c1})z^3 + 2\mu_c z^2 - (\Delta_{c1} + t_{c1})z - (\Delta_{c2} +$

$t_{c2}) = 0$ . Obviously, the Hamiltonian returns to Eq. (11) if one sets  $t_{c2} = \Delta_{c2} = 0$ . Fig. 5 depicts the relation between the coupling strength and the parameters of the central chain. One observes that the analytical solutions are in well agreement with the numerical solutions when  $\mu_c \gg t_c$ , i.e.,  $E_k \gg t_{1,2}$ . In the presence of long-range coupling, the coupling strength  $\epsilon$  is also enhanced since it takes minimum when  $t_{c2} = \Delta_{c2} = 0$ , as shown in Fig. 5(b). The results are not surprising since there are multiple channels for electrons co-tunneling in the long-range coupling regime, i.e., the NNN hopping amplitude also makes contributions to the electrons co-tunneling process.

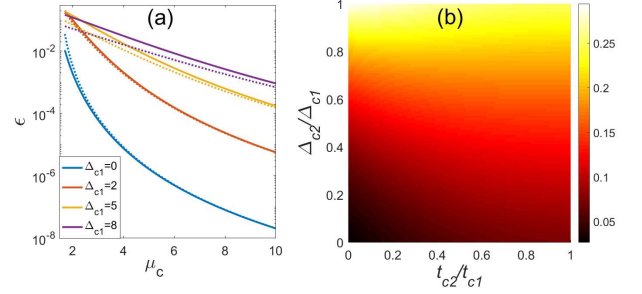


FIG. 5: (a) The coupling strength  $\epsilon$  as a function of the chemical potential  $\mu_c$ .  $N = 10$ .  $t_{c2} = \frac{1}{2}t_{c1}$ .  $\Delta_{c2} = \frac{1}{2}\Delta_{c1}$ .  $t_1 = t_2 = t_{c1}$ .  $t'_1 = t'_2 = t_{c2}$ . The solid line and dot line denote the exact numerical solutions and the approximate analytical solutions, respectively. (b) The coupling strength  $\epsilon$  as a function of the hopping amplitude and pairing amplitude.  $\mu_c = 2$ .  $\Delta_{c1} = 5$ .

#### IV. MODULATION OF CMBS BY PERIODIC DRIVING

As shown in Sec. II, CMBS is closely related to the chemical potential, the hopping amplitude, and the pairing amplitude of the central chain [cf. Eq. (11)], which implies that we can modulate the coupling strength  $\epsilon$  by varying the values of those parameters. Considering the hopping amplitude and the pairing amplitude cannot be easily manipulated in practice, we first explore the relation between the coupling strength  $\epsilon$  and the chemical potential  $\mu_c$ . Here, we do not intend to plot directly the dependence of  $\epsilon$  on  $\mu_c$ . Instead, we show the dependence of Rabi oscillation between two MBSs on  $\mu_c$ . By revealing different values of Rabi frequency, it can show not only how the coupling strength changes with the chemical potential [since distinct coupling strengths can reflect on distinct Rabi frequencies, cf. Eq. (24)], but also how well the Majorana qubit works.

To demonstrate Rabi oscillation, we first write down the total Hamiltonian of inhomogeneous chain in the BdG form:  $H_{total} = \frac{1}{2}A^\dagger \mathcal{H}_{total} A$ , where the basis  $A = [a_{-N_1}, \dots, a_{N_2}, a_{-N_1}^\dagger, \dots, a_{N_2}^\dagger]^T$ . In fact, the MBSs is the eigenstates of BdG Hamiltonian  $\mathcal{H}_{total}$  corresponding

to zero eigenvalue. Suppose that the inhomogeneous chain is initially prepared in the left MBS  $\gamma_{-1}$ , i.e.,  $|\Psi(0)\rangle = \frac{1}{\sqrt{2}}(|-1\rangle + |\mathcal{N}\rangle)$ . Here, the label  $|m\rangle$  denotes the vector with components  $|m\rangle_j = \delta_{mj}$  in the basis  $A$ ,  $m, j \in \{-N_1, \dots, 2\mathcal{N}\}$ , and  $\mathcal{N}$  denotes the total number of sites. With these notations, the dynamics of inhomogeneous chain is governed by following equation [30]

$$i \frac{d|\Psi(t)\rangle}{dt} = \mathcal{H}_{total} |\Psi(t)\rangle, \quad (17)$$

In Fig. 6, we plot the population of  $|\Psi(0)\rangle$  (i.e., the left MBS  $\gamma_{-1}$ ) as a function of evolution time. If there does not exist CMBS, the Rabi oscillation can not appear in the system, as depicted in Fig. 6(a). In Figs. 6(b)-(d), different chemical potentials  $\mu_c$  result in different Rabi frequencies. When the chemical potential is large, the coupling strength would be small, leading to a small Rabi frequency. That is, the Rabi frequency increases with the decreasing of the chemical potential. Similarly, one can modulate the coupling strength by changing the pairing amplitude, as the blue-dark lines show in Fig. 7. Besides, the coupling strength can also be modulated purely by the phase of pairing amplitude, e.g., Refs. [25, 31–33].

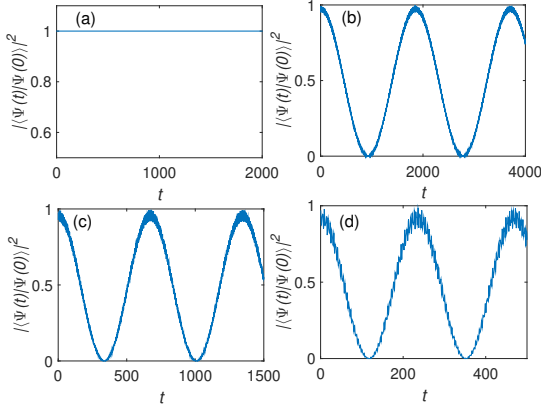


FIG. 6: Population of  $|\Psi(0)\rangle$  as a function of evolution time. The system is in the MBS  $\gamma_{-1}$  initially. The other parameters are  $\mathcal{N} = 20$ ,  $\mu_l = \mu_r = 0$ ,  $\Delta_l = \Delta_r = t_l = t_r = 5$ ,  $\Delta_c = 5$ ,  $t_1 = t_2 = t_c$ ,  $N = 10$ . (a)  $\mu_c = 10$ . (b)  $\mu_c = 3$ . (c)  $\mu_c = 2.5$ . (d)  $\mu_c = 2$ .

Since the pairing amplitude is inherently determined by the property of superconductors, it may be difficult to directly modulate with current techniques. In following we show that this goal can be reached by periodically driving the central chain, and the Hamiltonian of periodic driving field reads

$$H_\mu(t) = \mu_0 \cos \omega t \sum_{n=0}^N a_n^\dagger a_n, \quad (18)$$

where  $\mu_0$  and  $\omega$  are the amplitude and the frequency of the periodic driving field, respectively. In a realistic situation, this driving field can be achieved by applying

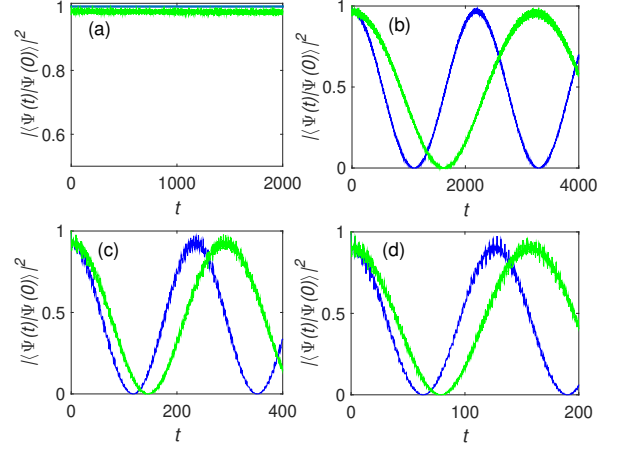


FIG. 7: Population of  $|\Psi(0)\rangle$  as a function of evolution time. The system is in the MBS  $\gamma_{-1}$  initially. The other parameters are  $\mu_l = \mu_r = 0$ ,  $\Delta_l = \Delta_r = t_l = t_r = 5$ ,  $\mu_c = 2$ ,  $t_1 = t_2 = t_c$ ,  $N = 10$ . (a)  $\Delta_c = 0$ . (b)  $\Delta_c = 2$ . (c)  $\Delta_c = 5$ . (d)  $\Delta_c = 10$ . The blue-dark lines are the exact numerical results obtained by Eq. (1), and the green-grey lines are plotted by the Hamiltonian given in Eq. (19). The effective pairing amplitude are the same for two lines in each panels.

an external ac electric potential to TLGV, since the on-site chemical potential can be modulated by TLGV.

At first, in the rotation frame defined by the unitary transformation,  $U(t) = e^{-i\frac{\mu_0}{\omega} \sin \omega t \sum_{n=0}^N a_n^\dagger a_n}$ , the effective Hamiltonian of the whole chain reads,

$$\begin{aligned} H'_{total} &= U^\dagger(t)[H_{total} + H_\mu(t)]U(t) - iU^\dagger(t)\dot{U}(t), \\ &= H_l + H_r + H'_c + H'_{lc} + H'_{rc}, \\ H'_c &= \sum_{n=0}^N \mu_c a_n^\dagger a_n - \sum_{n=0}^{N-1} \left( \frac{t_c}{2} a_n^\dagger a_{n+1} \right. \\ &\quad \left. + e^{i\frac{2\mu_0}{\omega} \sin(\omega t)} \frac{\Delta_c}{2} a_n^\dagger a_{n+1}^\dagger + h.c. \right), \\ H'_{lc} &= -e^{-i\frac{\mu_0}{\omega} \sin(\omega t)} \frac{t_1}{2} a_{-1}^\dagger a_0 + h.c., \\ H'_{rc} &= -e^{-i\frac{\mu_0}{\omega} \sin(\omega t)} \frac{t_2}{2} a_{N+1}^\dagger a_N + h.c., \end{aligned} \quad (19)$$

where  $H_l$  and  $H_r$  are invariant under this rotation. By making use of the identity

$$e^{ix \sin \omega t} = \sum_{n=-\infty}^{\infty} \mathcal{J}_n(x) e^{in\omega t}, \quad (20)$$

where  $\mathcal{J}_n(x)$  is the  $n$ -order Bessel function, the time-dependent effective Hamiltonian in the high-frequency

limit (i.e.,  $\omega \gg \mu_c, t_c$ ) becomes

$$\begin{aligned}
H'_c &= \sum_{n=0}^N \mu_c a_n^\dagger a_n - \sum_{n=0}^{N-1} \left( \frac{t_c}{2} a_n^\dagger a_{n+1} \right. \\
&\quad \left. + \frac{\Delta_c}{2} \mathcal{J}_0\left(\frac{2\mu_0}{\omega}\right) a_n^\dagger a_{n+1}^\dagger + h.c. \right), \\
H'_{lc} &= -\frac{t_1}{2} \mathcal{J}_0\left(\frac{\mu_0}{\omega}\right) a_{-1}^\dagger a_0 + h.c., \\
H'_{rc} &= -\frac{t_2}{2} \mathcal{J}_0\left(\frac{\mu_0}{\omega}\right) a_{N+1}^\dagger a_N + h.c.
\end{aligned} \tag{21}$$

One finds from Eq. (21) that the pairing amplitude of central chain is modulated by the amplitude and the frequency of driving field through zero-order Bessel function, i.e.,  $\Delta_{eff} = \frac{\Delta_c}{2} \mathcal{J}_0\left(\frac{2\mu_0}{\omega}\right)$ . In the presence of driving field, we plot the time evolution of the MBSs by the green-grey lines in Fig. 7. The results show that, even though the effective pairing amplitude with driving field equals to the pairing amplitude without driving field, the Rabi frequency is still a bit different in two cases. This originates from the fact that the effective hopping amplitudes at boundaries are also changed by driving field [see the expressions of  $H'_{lc}$  and  $H'_{rc}$  in Eq. (21)], rendering the correction of Rabi frequency. We would like to address that, this correction does not make difference for UMQR as it only changes evolution time to complete corresponding operations. Interestingly, we can also modulate the effective hopping amplitude at boundaries by driving field to control CMBS. It is demonstrated in Fig. 8(a) that the adjacent MBSs  $\gamma_{-1}$  and  $\gamma'_{N+1}$  are decoupled by making the effective hopping amplitude at boundaries ( $H'_{lc}$  and  $H'_{rc}$ ) vanish, i.e., setting  $\mathcal{J}_0\left(\frac{\mu_0}{\omega}\right) = 0$ . Otherwise, CMBS can be really induced, manifesting in the Rabi oscillation shown in Figs. 8(b)-(d).

## V. DISCUSSION AND CONCLUSION

As well known, an ordinary spinless fermion can be used to encode a logical qubit because it can span a two-dimensional Hilbert space (occupy or empty). However it is not true for MBSs since the operators satisfy  $\gamma_i = \gamma_i^\dagger$  and  $\gamma_i^2 = 1$ . By recombining the operators  $\gamma_i$ , one can use two MBSs to construct a Dirac fermion, e.g.,  $d_1 = \frac{1}{2}(\gamma'_{N_1} + i\gamma_{-1})$  and  $d_2 = \frac{1}{2}(\gamma'_{N+1} + i\gamma_{N_2})$  in Fig. 1. It seems that a logical qubit can be encoded by two MBSs now. Nevertheless, for the system with parity conservation (calculated through the Dirac fermions formed by MBSs), the coherent superposition of MBSs with different parities is prohibited. Therefore a logical qubit cannot be encoded by two MBSs in the parity conservation system. To guarantee two computational bases having same parity, four MBSs is necessary (see  $\gamma'_{N_1}$ ,  $\gamma_{-1}$ ,  $\gamma'_{N+1}$ , and  $\gamma_{N_2}$  in Fig. 1). For instance, we can construct the Majorana-based qubit in the odd parity subspace,

$$|1_1 0_2\rangle = d_1^\dagger |0_1 0_2\rangle, |0_1 1_2\rangle = d_2^\dagger |0_1 0_2\rangle, \tag{22}$$

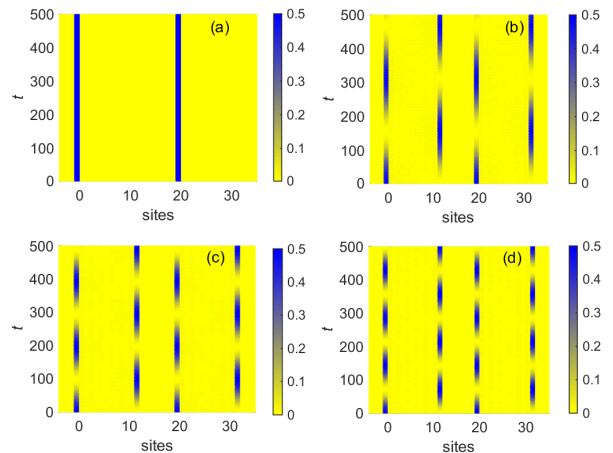


FIG. 8: The population of each sites in  $|\Psi\rangle$  as a function of time. The MBS  $\gamma_{-1}$  locates at the site  $-1$  initially.  $\Delta_c = 10$ .  $N = 20$ . (a)  $\mathcal{J}_0\left(\frac{\mu_0}{\omega}\right) = 0$ . (b)  $\mathcal{J}_0\left(\frac{\mu_0}{\omega}\right) = 0.8605$ . (c)  $\mathcal{J}_0\left(\frac{\mu_0}{\omega}\right) = 0.9120$ . (d)  $\mathcal{J}_0\left(\frac{\mu_0}{\omega}\right) = 0.9696$ . The other physical parameters are the same as in Fig. 7. The three part of Kitaev chain are decoupled from each other when  $\mathcal{J}_0\left(\frac{\mu_0}{\omega}\right) = 0$ , and there exists Rabi oscillation between the adjacent MBSs  $\gamma_{-1}$  and  $\gamma'_{N+1}$  when  $\mathcal{J}_0\left(\frac{\mu_0}{\omega}\right) \neq 0$ , where the MBSs  $\gamma'_{N+1}$  locates at site 11.

where  $|0_1 0_2\rangle$  is the vacuum state of Dirac fermions. The topologically protected single qubit operations are achieved by exchanging spatial positions of the MBSs  $\gamma'_{N_1}$  and  $\gamma_{-1}$ , which exhibit the non-Abelian statistics. This braiding operation, i.e., the  $\frac{\pi}{4}$  phase gate, is represented by the following unitary operation

$$U_{N_1 0} = e^{\frac{i\pi}{4}\sigma_z}, \tag{23}$$

where  $\sigma_z = |1_1 0_2\rangle\langle 1_1 0_2| - |0_1 1_2\rangle\langle 0_1 1_2|$ . This process can be realized in the one-dimensional semiconducting wires with T-junction by controlling TLGV adiabatically [25]. Note that the braiding operation is insufficient for realizing universal quantum computation since it is not able to perform arbitrary single qubit rotations [2, 34], which are usually not topologically protected (rotation angle  $\theta \neq \frac{\pi}{2}n$ ,  $n$  is integer).

When there exists CMBS in the system (it has been also investigated in the continuous model instead of lattice model [35–41]), the effective Hamiltonian takes  $H_{0N} = \frac{i\epsilon}{2}\gamma_{-1}\gamma'_{N+1}$ . We can obtain the following unitary operation for a fixed evolution time

$$U_{0N}(t) = e^{-\frac{i\epsilon t}{2}\sigma_x}, \tag{24}$$

where  $\sigma_x = |1_1 0_2\rangle\langle 0_1 1_2| + |0_1 1_2\rangle\langle 1_1 0_2|$ . Together with the braiding operation  $U_{N_1 0}$ , one can implement UMQR via the successive operations  $U' = U_{0N}(t_2)U_{N_1 0}U_{0N}(t_1)$  [18]. To realize the operation  $U'$ , exact control over CMBS with a fixed evolution time is required. This is crucial since the procedure is usually not topologically protected. The other consideration is that the MBSs should decouple instantaneously from each other after (before) the

coupling of the adjacent MBSs. As shown in Figs. (6)-(8), the two considerations are sufficiently solved since the modulation of the amplitude or frequency of the electric potential on TLGV can be controlled with high precision. For example, in order to manipulate the chemical potential, we adopt two distinct voltages, e.g.,  $\mu_{c1} = 10$  and  $\mu_{c2} = 2.5$  as shown in Fig. 6(a) and Fig. 6(c). We first apply a low voltage  $\mu_{c2}$  for periods of time  $t_1$  to realize the operation  $U_{0N}(t_1)$ . Then we switch it to a high voltage  $\mu_{c1}$  to realize the braiding operation  $U_{N_1 0}$ . Next we change the gate to the low voltage  $\mu_{c2}$  for periods of time  $t_2$  to realize the operation  $U_{0N}(t_2)$ . Finally we take back to the high voltage  $\mu_{c1}$  to cancel CMBS. This suggests that UMQR can be realized by changing TLGV in a square-wave form, composed by  $\mu_{c1}$  and  $\mu_{c2}$ . In fact, the results are the same as in the case where the driving frequency is switched to  $\omega_1$  or  $\omega_2$  in sequence; see Fig. 8(a) and Fig. 8(c).

In conclusion, we have studied CMBS in the inhomogeneous Kitaev chain with short-range and long-range coupling. We demonstrate that CMBS depends sharply on the pairing amplitude and the chemical potential of the central chain. Particularly, CMBS is remarkably en-

hanced when existing the pairing amplitude or long-range coupling. In addition we have explored the dependence of CMBS on the frequency and amplitude of the driving field. These results suggest that there are many ways to change CMBS such as manipulating the chemical potential of central chain, or modulating the effective pairing amplitude of central chain which can be realized by changing the frequency (or amplitude) of driving field. Finally, we have demonstrated the application of tunable CMBS, i.e., implementing unitary rotation operations for quantum computation.

## ACKNOWLEDGMENTS

This work is supported by the National Natural Science Foundation of China (Grant Nos. 11575045, 11374054, 11674060, 11534002, and 61475033), the Major State Basic Research Development Program of China under Grant No. 2012CB921601, and the fund from Fuzhou University under No. XRC-1639.

- 
- [1] A. Y. Kitaev, *Ann. Phys.* **303**, 2 (2003).
  - [2] C. Nayak, S. H. Simon, A. Stern, M. Freedman, and S. Das Sarma, *Rev. Mod. Phys.* **80**, 1083 (2008).
  - [3] N. Read and D. Green, *Phys. Rev. B* **61**, 10267 (2000).
  - [4] D. A. Ivanov, *Phys. Rev. Lett.* **86**, 268 (2001).
  - [5] L. Fu and C. L. Kane, *Phys. Rev. Lett.* **100**, 096407 (2008).
  - [6] M. Z. Hasan and C. L. Kane, *Rev. Mod. Phys.* **82**, 3045 (2010).
  - [7] J. D. Sau, R. M. Lutchyn, S. Tewari, and S. Das Sarma, *Phys. Rev. Lett.* **104**, 040502 (2010).
  - [8] X. L. Qi and S. C. Zhang, *Rev. Mod. Phys.* **83**, 1057 (2011).
  - [9] J. Alicea, *Rep. Prog. Phys.* **75**, 076501 (2012).
  - [10] C. W. J. Beenakker, *Annu. Rev. Con. Mat. Phys.* **4**, 113 (2013).
  - [11] A. Das, Y. Ronen, Y. Most, Y. Oreg, M. Heiblum, and H. Shtrikman, *Nat. Phys.* **8**, 887 (2012).
  - [12] V. Mourik, K. Zuo, S. M. Frolov, S. R. Plissard, E. P. A. M. Bakkers, and L. P. Kouwenhoven, *Science*, **336**, 1003 (2012).
  - [13] M. T. Deng, C. L. Yu, G. Y. Huang, M. Larsson, P. Caroff, and H. Q. Xu, *Nano Lett.* **12**, 6414 (2012).
  - [14] L. P. Rokhinson, X. Liu, and J. K. Furdyna, *Nat. Phys.* **8**, 795 (2012).
  - [15] S. N. Perge, I. K. Drozdov, J. Li, H. Chen, S. Jeon, J. Seo, A. H. MacDonald, B. A. Bernevig, and A. Yazdani, *Science*, **346**, 602 (2014).
  - [16] E. J. H. Lee, X. Jiang, M. Houzet, R. Aguado, C. M. Lieber, and S. De Franceschi, *Nat. Nanotech.* **9**, 79 (2014).
  - [17] T. L. Schmidt, A. Nunnenkamp, and C. Bruder, *Phys. Rev. Lett.* **110**, 107006 (2013).
  - [18] T. L. Schmidt, A. Nunnenkamp, and C. Bruder, *New J. Phys.* **15**, 025043 (2013).
  - [19] A. Yu. Kitaev, *Phys. Usp.* **44**, 131 (2001).
  - [20] E. Lieb, T. Schultz, and D. Mattis, *Ann. Phys. (NY)* **16**, 407 (1961).
  - [21] Y. Oreg, G. Refael, and F. von Oppen, *Phys. Rev. Lett.* **105**, 177002 (2010).
  - [22] R. M. Lutchyn, J. D. Sau, and S. D. Sarma, *Phys. Rev. Lett.* **105**, 077001 (2010).
  - [23] S. Nadj-Perge, I. K. Drozdov, J. Li, H. Chen, S. Jeon, J. Seo, A. H. MacDonald, B. A. Bernevig, and A. Yazdani, *Science* **346**, 602 (2014).
  - [24] R. Pawlak, M. Kisiel, J. Klinovaja, T. Meier, S. Kawai, T. Glatzel, D. Loss, and E. Meyer, arXiv:1505.06078.
  - [25] J. Alicea, Y. Oreg, G. Refael, F. von Oppen, and M. P. A. Fisher, *Nat. Phys.* **7**, 412 (2011).
  - [26] C. J. Bolech and E. Demler, *Phys. Rev. Lett.* **98**, 237002 (2007).
  - [27] J. R. Schrieffer and P. A. Wolff, *Phys. Rev.* **149**, 491 (1966).
  - [28] L. Jiang, T. Kitagawa, J. Alicea, A. R. Akhmerov, D. Pekker, G. Refael, J. I. Cirac, E. Demler, M. D. Lukin, and P. Zoller, *Phys. Rev. Lett.* **106**, 220402 (2011).
  - [29] C. V. Kraus, S. Diehl, P. Zoller, and M. A. Baranov, *New J. Phys.* **14**, 113036 (2012).
  - [30] P. G. de Gennes, *Superconductivity of Metals and Alloys* (W. A. Benjamin, New York, 1966).
  - [31] A. A. Zyuzin, D. Rainis, J. Klinovaja, and D. Loss, *Phys. Rev. Lett.* **111**, 056802 (2013).
  - [32] Q. J. Tong, J. H. An, J. B. Gong, H. G. Luo, and C. H. Oh, *Phys. Rev. B* **87**, 201109 (2013).
  - [33] Z. Y. Xue, M. Gong, J. Liu, Y. Hu, S. L. Zhu, and Z. D. Wang, *Sci. Rep.* **5**, 12233 (2015).
  - [34] S. Bravyi, *Phys. Rev. A* **73**, 042313 (2006).
  - [35] M. Cheng, R. M. Lutchyn, V. Galitski, and S. Das Sarma,

- Phys. Rev. Lett. **103**, 107001 (2009).
- [36] J. D. Sau, D. J. Clarke, and S. Tewari, Phys. Rev. B **84**, 094505 (2011).
- [37] S. D. Sarma, J. D. Sau, and T. D. Stanescu, Phys. Rev. B **86**, 220506 (2012).
- [38] E. Prada, P. S. Jose, and R. Aguado, Phys. Rev. B **86**, 180503 (2012).
- [39] D. Rainis, L. Trifunovic, J. Klinovaja, and D. Loss, Phys. Rev. B **87**, 024515 (2013).
- [40] A. Cottet, T. Kontos, and B. Douçot, Phys. Rev. B **88**, 195415 (2013).
- [41] A. A. Kovalev, A. De, and K. Shtengel, Phys. Rev. Lett. **112**, 106402 (2014).